Cosmic-Ray Propagation Properties for an Origin in Supernova Remnants

I. Büsching, A. Kopp, M. Pohl, R. Schlickeiser, C. Perrot , I. Grenier

Astrophysical Journal, 619:314-326, 2005

ICRR CANGAROO group internal seminar, December 19, 2005

Time-dependent propagation model for CR nucleons

- Would a SNR origin of CR nucleons also lead to significant fluctuations of the CR density in the Galaxy, which then would modify secondary-to-primary ratios from their steady state values? If this was the case, we would have to rethink the way we infer CR propagation parameters from their locally observed spectra.
- Are there any signatures in the CR distribution in the Galaxy that might permit us to infer an SNR origin of CR nucleons on the grounds of locally observed CR spectra and the diffuse Galactic γ-ray emission?

Cf. Electron spectra variation may explain diffuse gamma-ray “GeV bump”

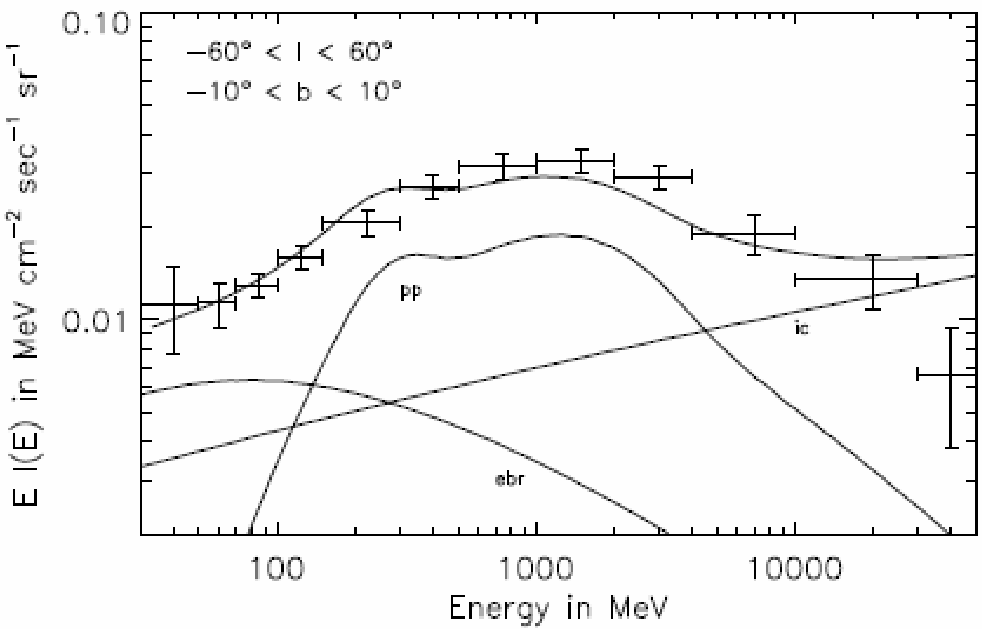

Fig. 5.—Gamma-ray intensity in the direction of the inner Galaxy. The data points are taken from Hunter et al. (1997). The error bars include an estimate for the systematic error of 8%, which accounts for the uncertainty in the energy-dependent correction of the spark chamber efficiency (Esposito et al. 1998). The data are compared with bremsstrahlung (“ebr”) and Inverse Compton (“ic”) spectra from our model, on the basis of sources with injection indexes following a normal distribution of mean 2.0 and dispersion 0.2 and the spatial distribution of SNRs in spiral arms. The π^0-component is a template and not a model.

Electron accelerated in SNR with power-law spectra of index -2.0 but varies by around 0.2

↓

Enhanced Inverse Compton

↓

“GeV bump” in diffuse gamma-rays

Pohl & Esposito, ApJ 507, 327 (1998)

The model

- Continuity equation

$$\frac{\partial N}{\partial t} - S = \nabla(k\nabla N) - \Omega v \sigma N,$$

σ: spallation cross section

- Interstellar gas profile

$$\Omega(z) = \frac{n_0}{\cosh(zh_g)}.$$

$$n_0 = 1.24 \ \mathrm{cm}^{-3} \ \text{and} \ h_g = 30 \ \mathrm{kpc}^{-1}$$

- Diffusion coefficient

$$k = \begin{cases} k_0\left(\frac{\zeta}{\zeta_0}\right)^{0.6} & \text{for } \zeta \geq \zeta_0 \\ k_0\left(\frac{\zeta}{\zeta_0}\right)^{-0.48} & \text{for } \zeta < \zeta_0 \end{cases},$$

$$\zeta_0 = 4 \ \mathrm{GV} \ c^{-1}$$

ζ: rigidity

- Source spectra

$$q_j(\zeta, t) = \hat{q}_j(t - t_j)\exp\left(-\frac{t - t_j}{20 \ \mathrm{kyr}}\right)\Theta(t - t_j)\left(\frac{\zeta}{\zeta_0}\right)^{-s}.$$

Linear growth with an exponential cutoff

- SNR distribution

$$\tilde{P}_S(r, z) = \frac{1}{\cosh(zh_g)}\left(\frac{br}{ar_s}\right)^a \exp\left(\frac{ar_s - br}{r_s}\right),$$

Case & Bhattacharya (1996)

25 SNe per Myr and kpc^2 of the Galactic disk

Diffusion term

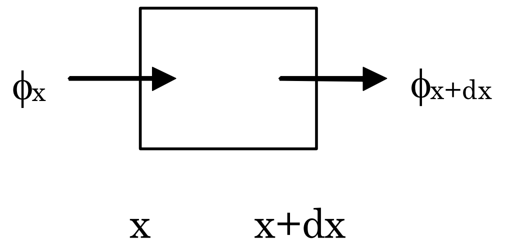

ϕ: particle flux

$$\frac{d}{dt}N(x,t)dx = [\phi_x(x,t) - \phi_x(x+dx,t)] + Q(x,t)dx$$

$$\frac{d}{dt}N(x,t) = -\frac{\partial}{\partial x}\phi_x(x,t) + Q(x,t)$$

$$\phi_x \equiv -k\frac{\partial N}{\partial x}$$

$$\therefore \frac{d}{dt}N(x,t) = \frac{\partial}{\partial x}\left(k\frac{\partial}{\partial x}\phi_x(x,t)\right) + Q(x,t)$$

SNR distribution

Case & Bhattacharya, A&AS 120, 437 (1996)

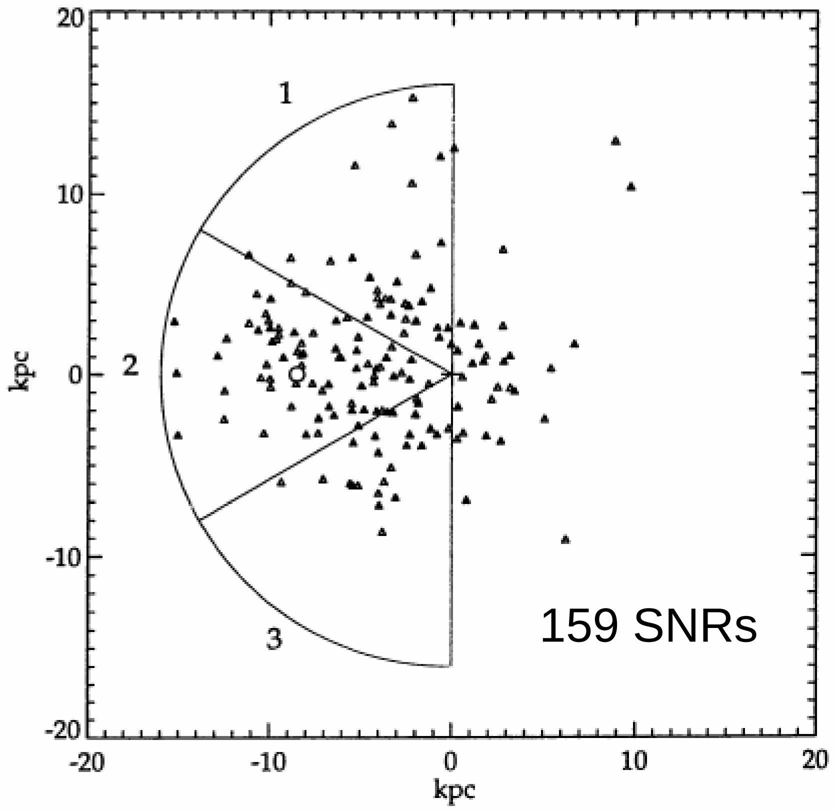

Fig. 1. The near half of the Galaxy is divided into three broad regions. The triangles represent the positions of the SNRs, while the "o" marks the position of the sun and the "+" marks the Galactic Center

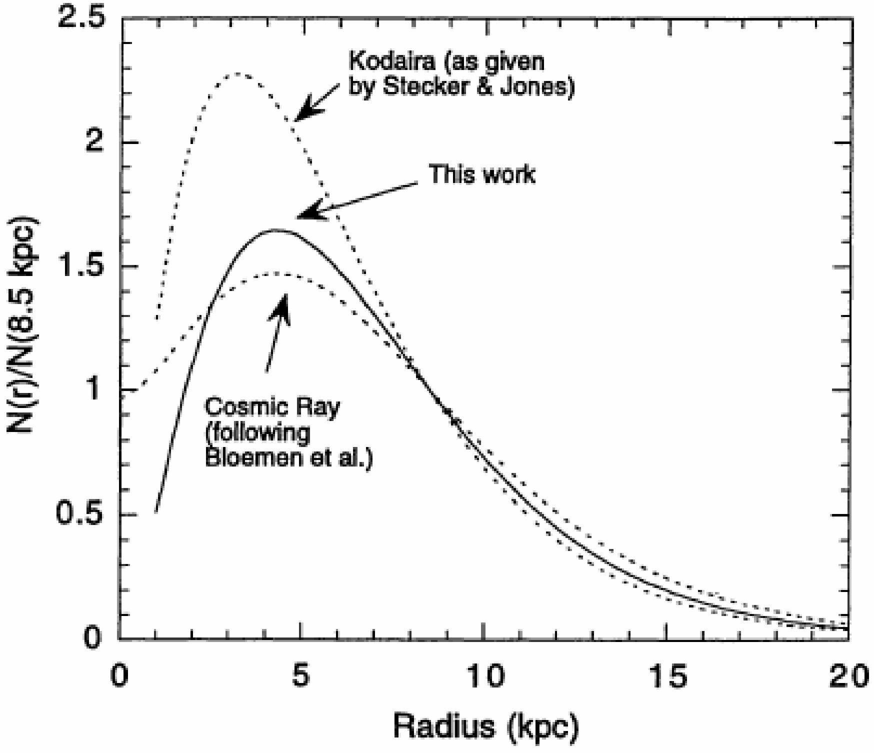

Fig. 3. The functional form of the SNR density distribution and the resulting cosmic ray distribution are shown. All curves are normalized to 8.5 kpc

Fig.1: Sketch of the geometry used in our calculations. We assume that the Galactic disk with radius *R*=20kpc is filled with interstellar gas and the CR sources. The density of the interstellar gas decreases quasi-exponentially in the halo. The height of the entire diffusion zone is 2*H*.

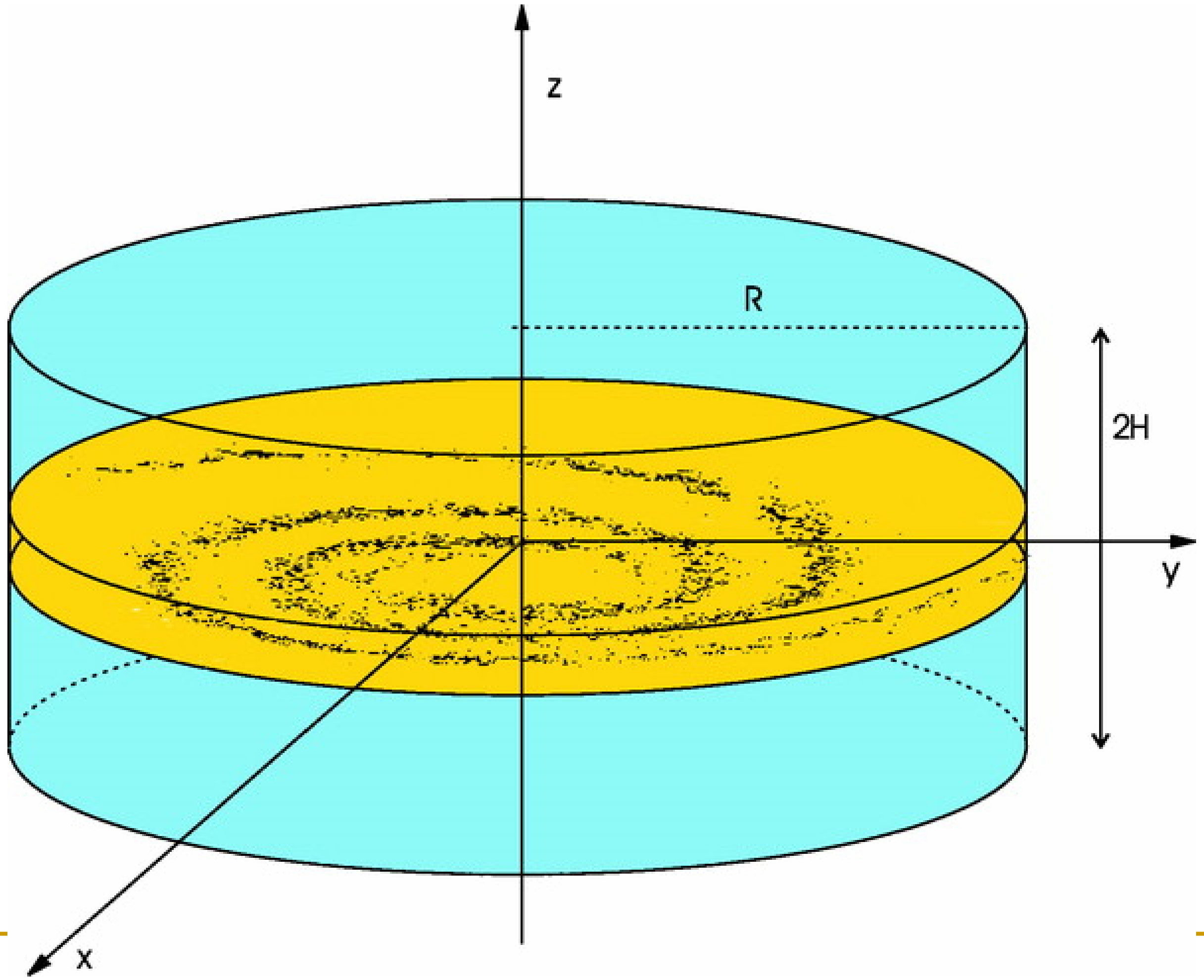

Fig.2: Best fits of boron-to-carbon data (*left*) and $^{10}Be/^{9}Be$ data (*right*), compared with data by Engelmann et al. (1990; *triangles*), Dwyer & Meyer (1987; *diamonds*), Krombel & Wiedenbeck (1988; *squares*), and Orth et al. (1978; *crosses*) for the boron-to-carbon ratio and from Connell (1998), Garcia-Munoz et al. (1981), Hams et al. (2001), Lukasiak et al. (1994), de Nolfo et al. (2001), and Wiedenbeck & Greiner (1980) for the ^{10}Be to ^{9}Be ratio.

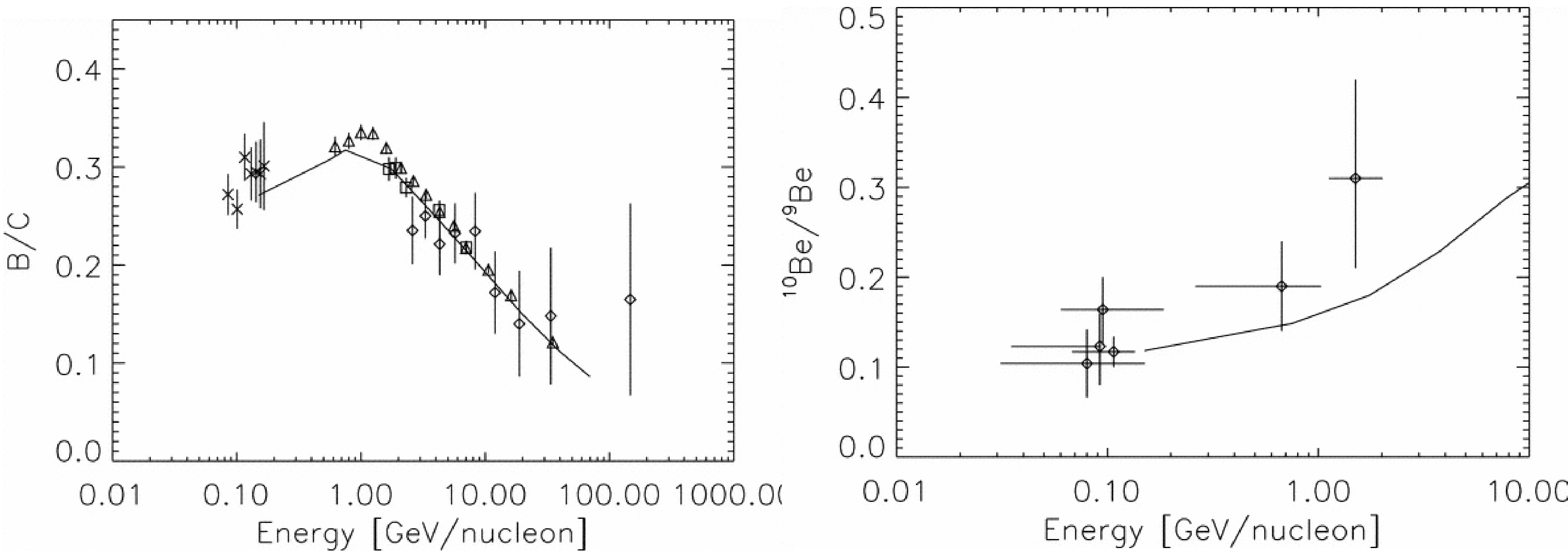

→ the best-fit parameters are $k_0 = 0.26$ kpc^2 Myr^{-1}, $H = 2$ kpc, and $s = 2.1$, as shown in Figure 2.

Calculation

- *(skipped…)*

$$N = \frac{1}{\pi}\sum_n \sum_m [A_{nm}\cos(n\varphi) + B_{nm}\sin(n\varphi)]\,\frac{J_n(\alpha_{nm} r)}{[J_n'(\alpha_{nm} R)]^2},$$

Fourier/Fourier-Bessel series expansion

- For a single source

$$\begin{aligned}
N(\rho,t) = \int_{t_0=0}^{t} \Bigg(& -2\sqrt{k(t-t_0)}\exp\left[\frac{-\rho_s^2-\rho^2}{4k(t-t_0)}\right] \\
& \times \sinh\left[\frac{\rho_s\rho}{2k(t-t_0)}\right]\rho^{-1} \\
& + \frac{\sqrt{\pi}}{2}\left\{\operatorname{erf}\left[\frac{1}{2}\frac{\rho_s-\rho}{\sqrt{k(t-t_0)}}\right]\right. \\
& \left. + \operatorname{erf}\left[\frac{1}{2}\frac{\rho_s+\rho}{\sqrt{k(t-t_0)}}\right]\right\}\Bigg) \\
& \times \exp[b(t_0-t)]\,t_0\exp\left(-\frac{t_0}{\tau}\right)dt_0.
\end{aligned}$$

Fig.3: Comparison of CR density due to a spherical source with radius 50 pc given by eq. (20) (*solid line*) with that computed using eq. (7) with 312 coefficients used for the series in *n* and 210 coefficients used in the series in *m*; cuts in the *r* (*dotted line*) and φ (*dashed line*) directions are shown for different times from source "ignition."

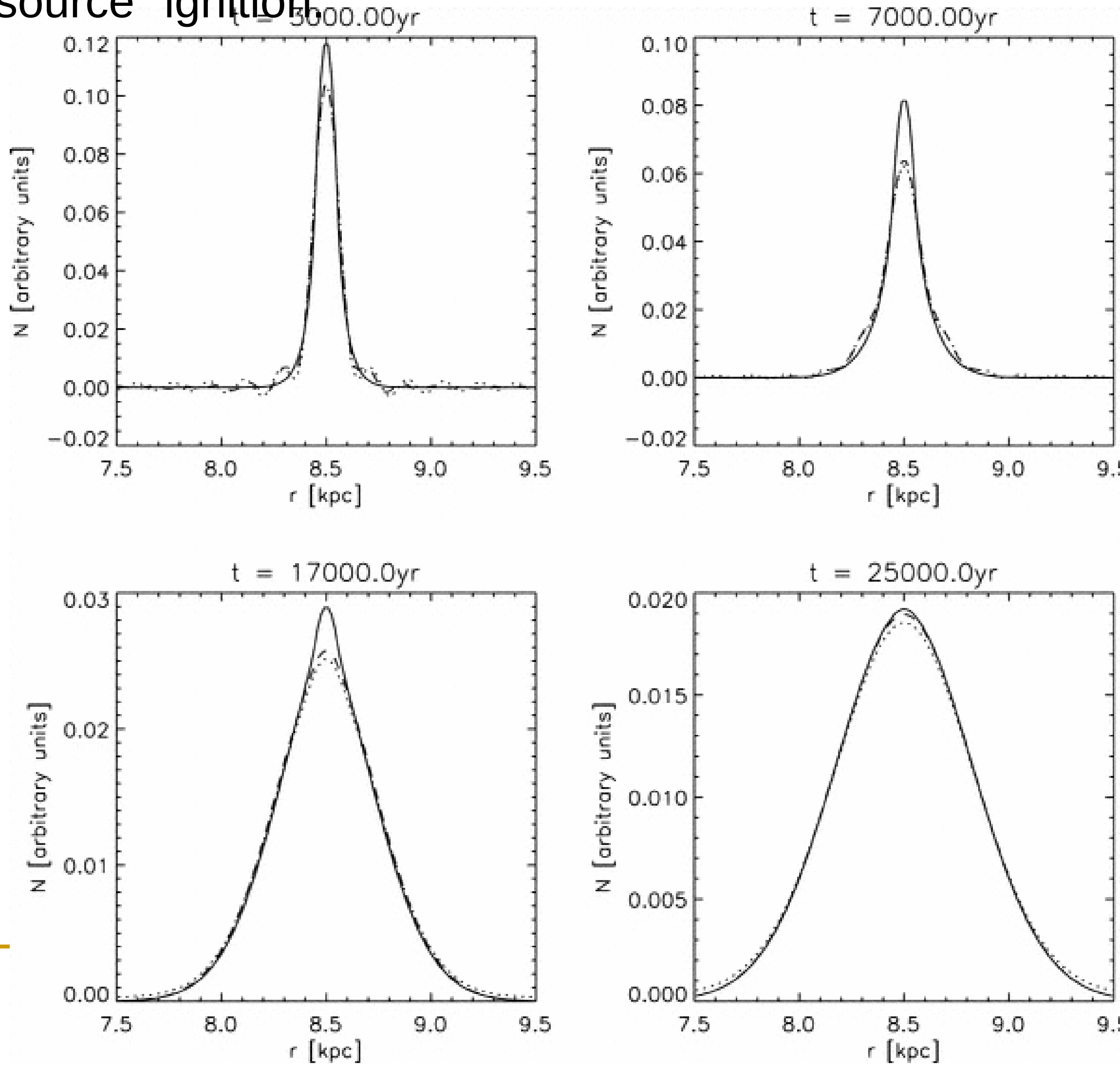

Fig.4: Temporal variation of the ^{16}O CR primary density at the position of the Sun, for 10 GeV/nucleon (left) and 5 TeV/nucleon (*right*).

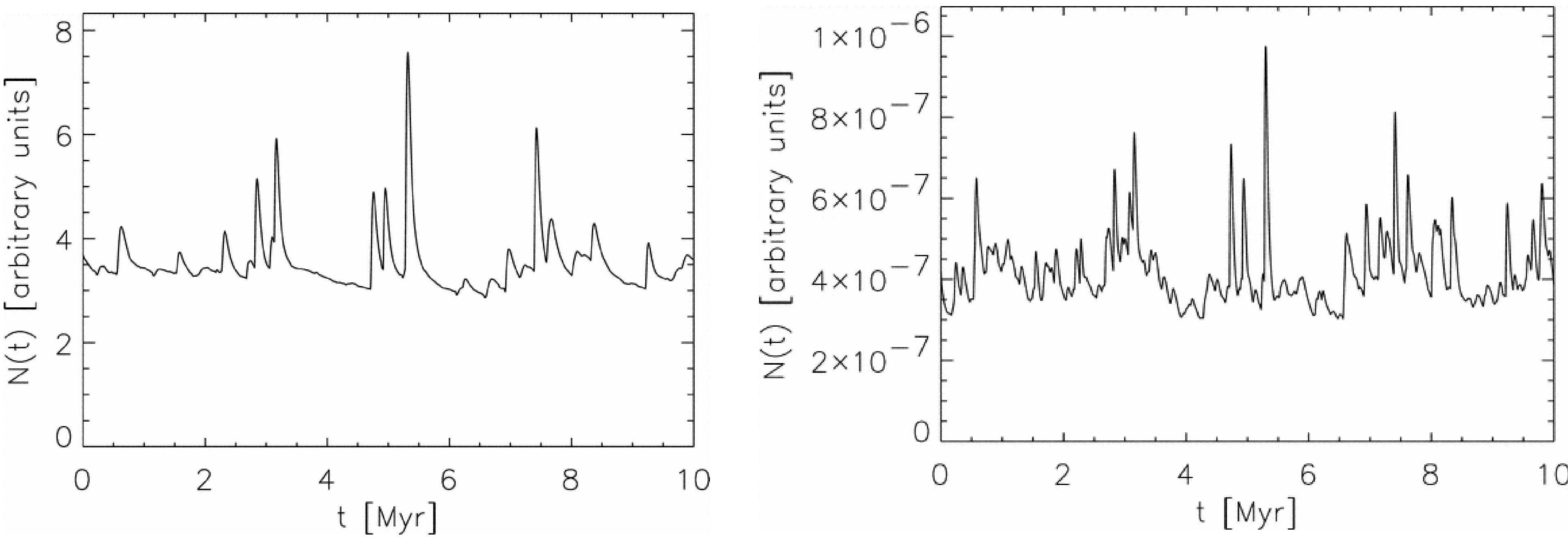

Fig.5: Density of ^{16}O at E = 10 GeV/nucleon in a 400 pc × 400 pc section of the Galactic plane (z = 0) during a local SN event for several times (in Myr). The Sun (r = 8.5 kpc, ϕ = 1.025) is positioned at the center. The local CR density is strongly influenced by nearby SNe, although the excess quickly disappears.

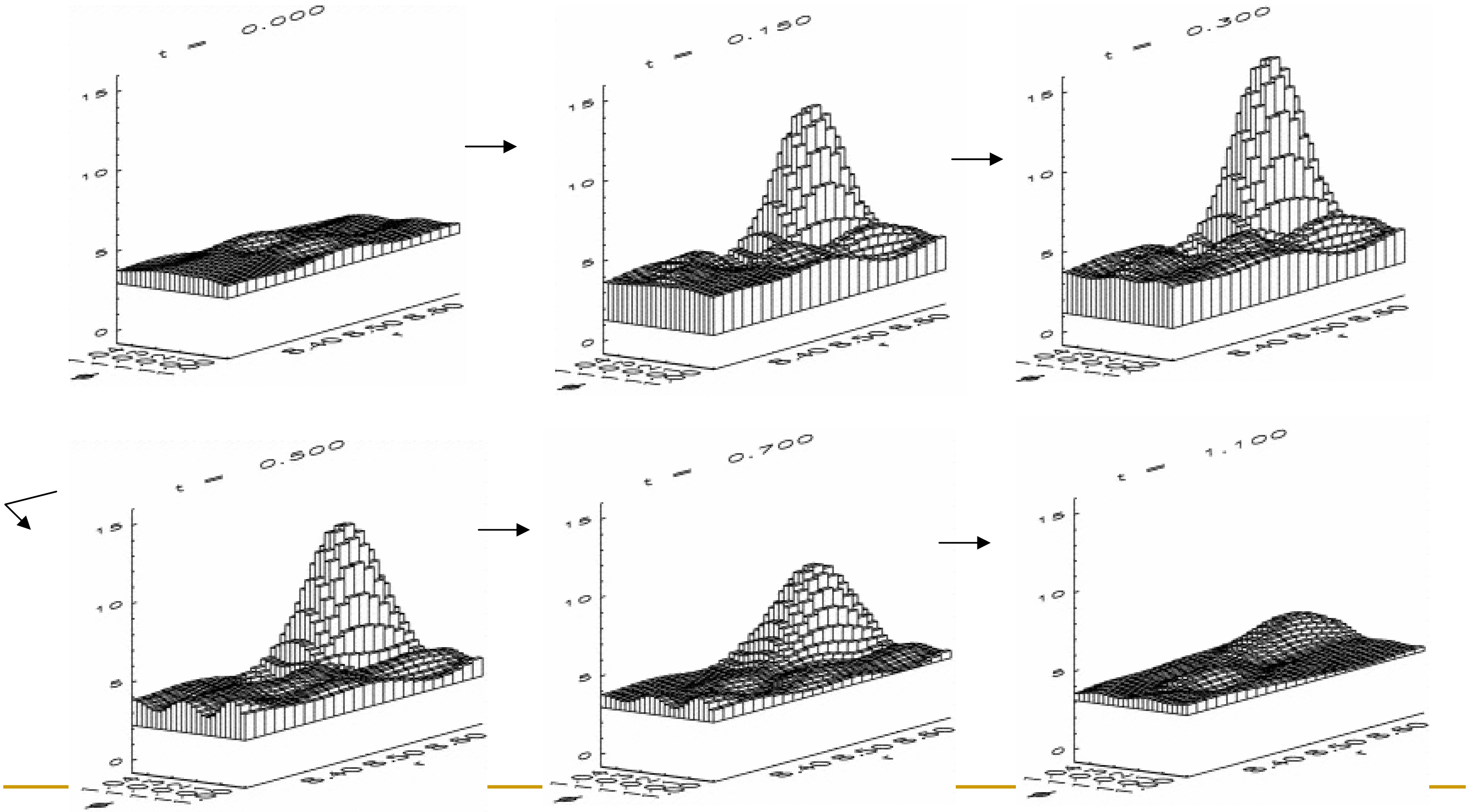

Fig.6: Same as Fig. 4, but assuming a locally enhanced SN rate in the Gould Belt.

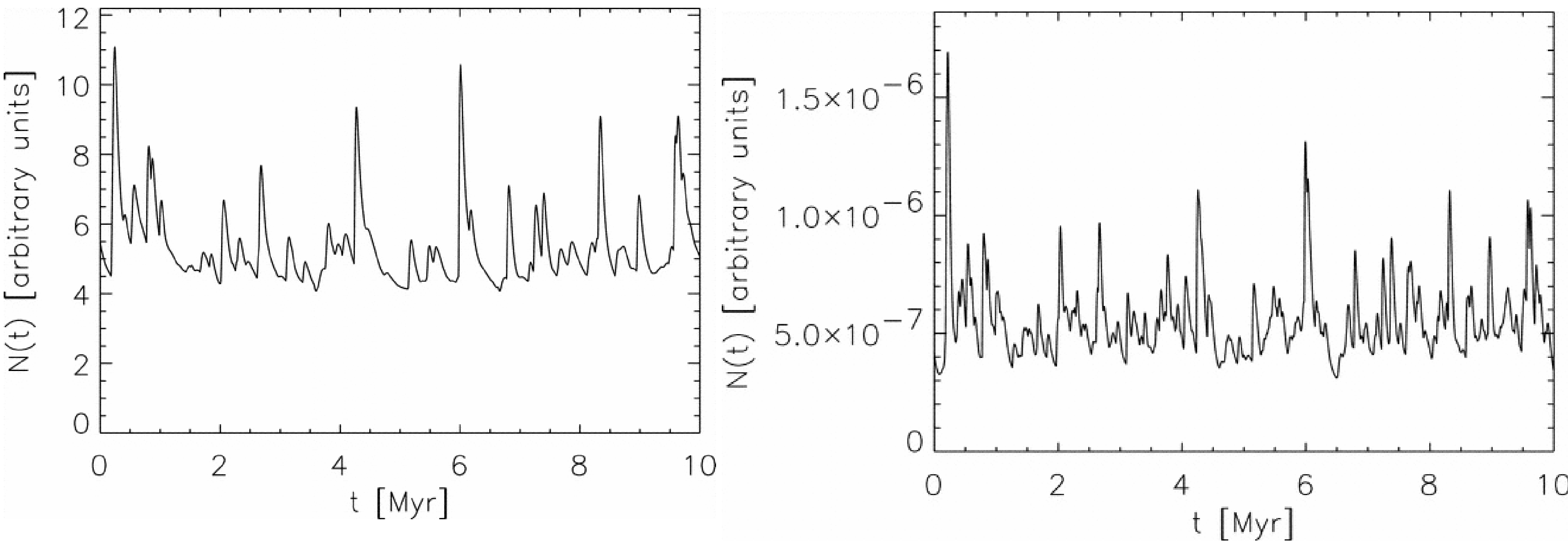

Fig.7: Temporal variation of the CR primary density ^{12}C (*left*) and secondary ^{11}B (*right*) at the position of the Sun at an energy of 10 GeV/nucleon. The deviation from the average value for the CR secondary density is far smaller than that for the CR primary density.

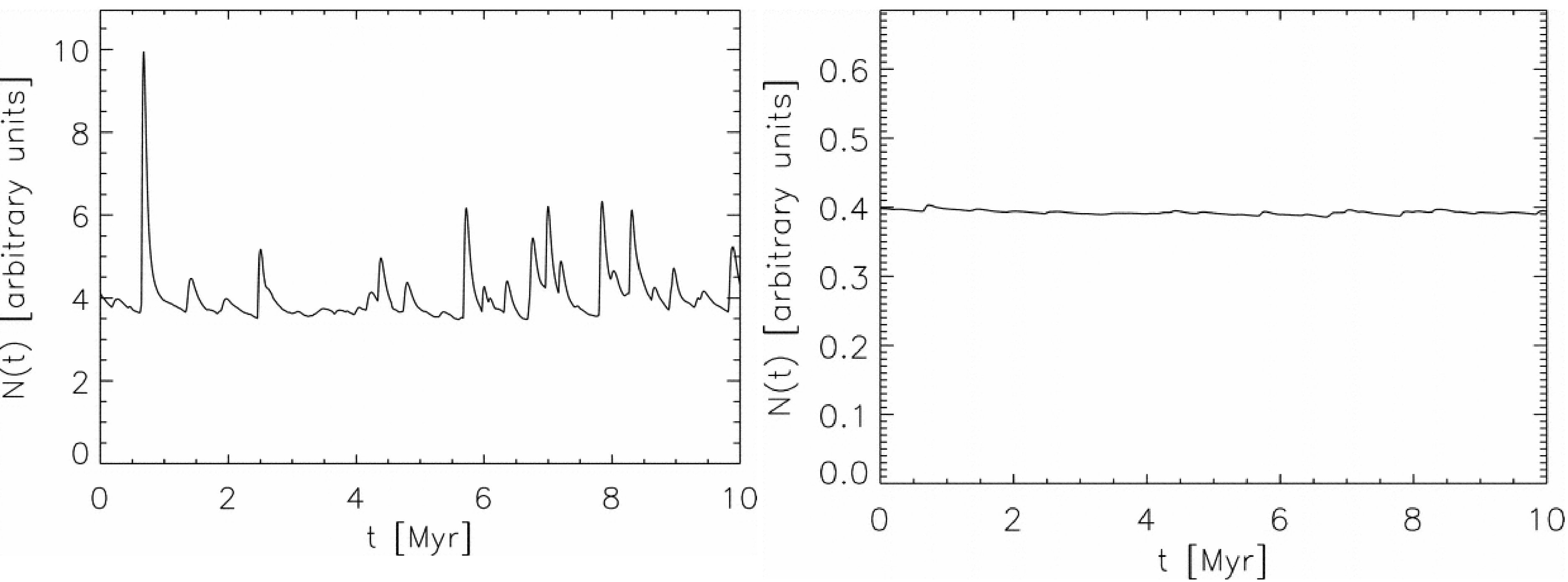

Fig.8: Density of primary CRs (*upper panels*) and secondary CRs (*lower panels*) plotted as a function of distance from the Galactic plane at R_0 = 8.5 kpc from the Galactic center. The left panels are for a particle energy of 10 GeV/nucleon and the right panels apply to particles at an energy of 5 TeV. We show the density distributions at four arbitrarily chosen instances of time, indicated by different line styles.

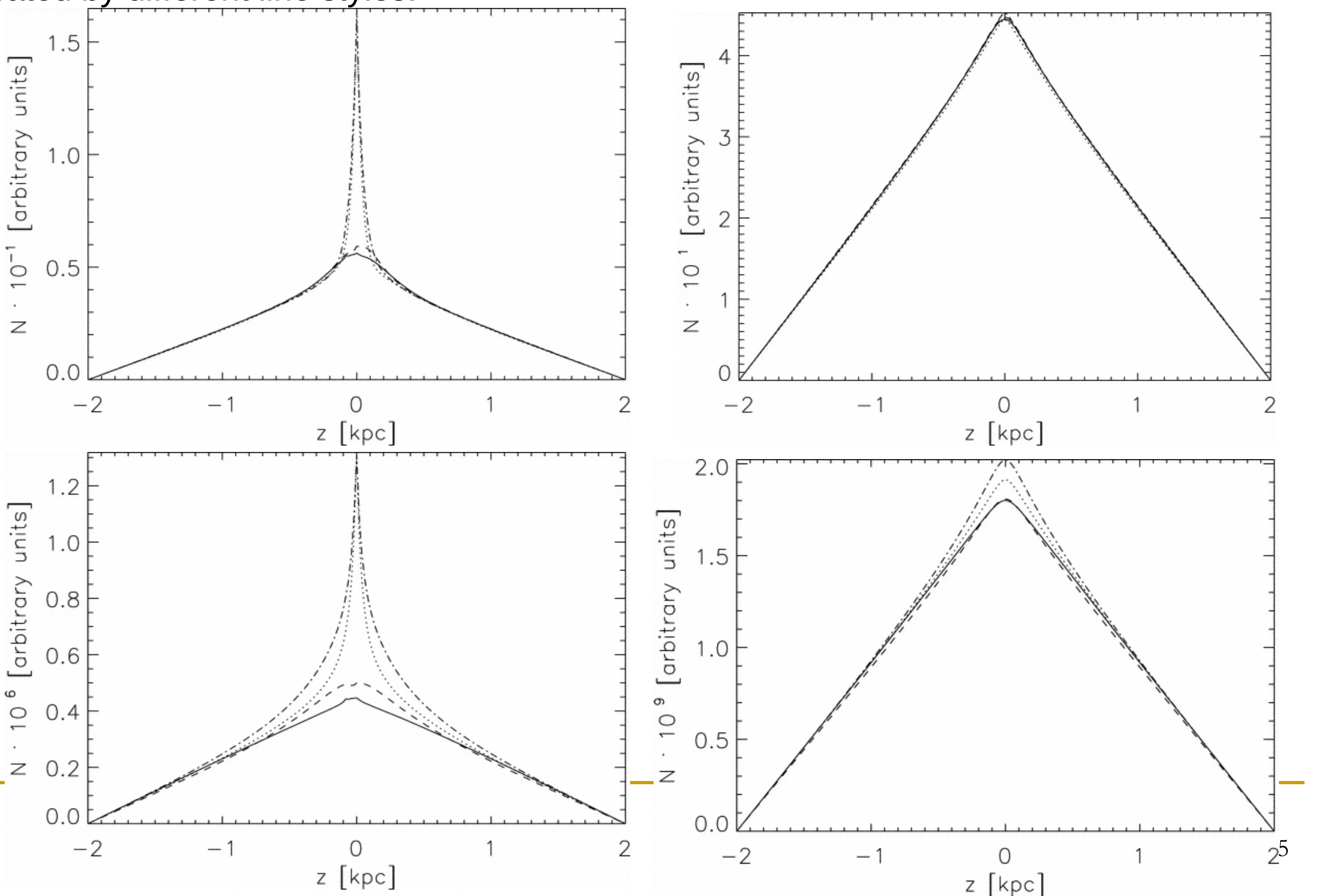

Fig.9: Range of possible ^{16}O spectra with (*left*) and without (*right*) the Gould Belt compared with measurements taken with balloons or satellites. The dark gray band shows the 68% containment probability range at each given energy and the light gray band gives the 95% range. The solid line marks the averaged (steady state) spectrum. All spectra are as at the top of the atmosphere.

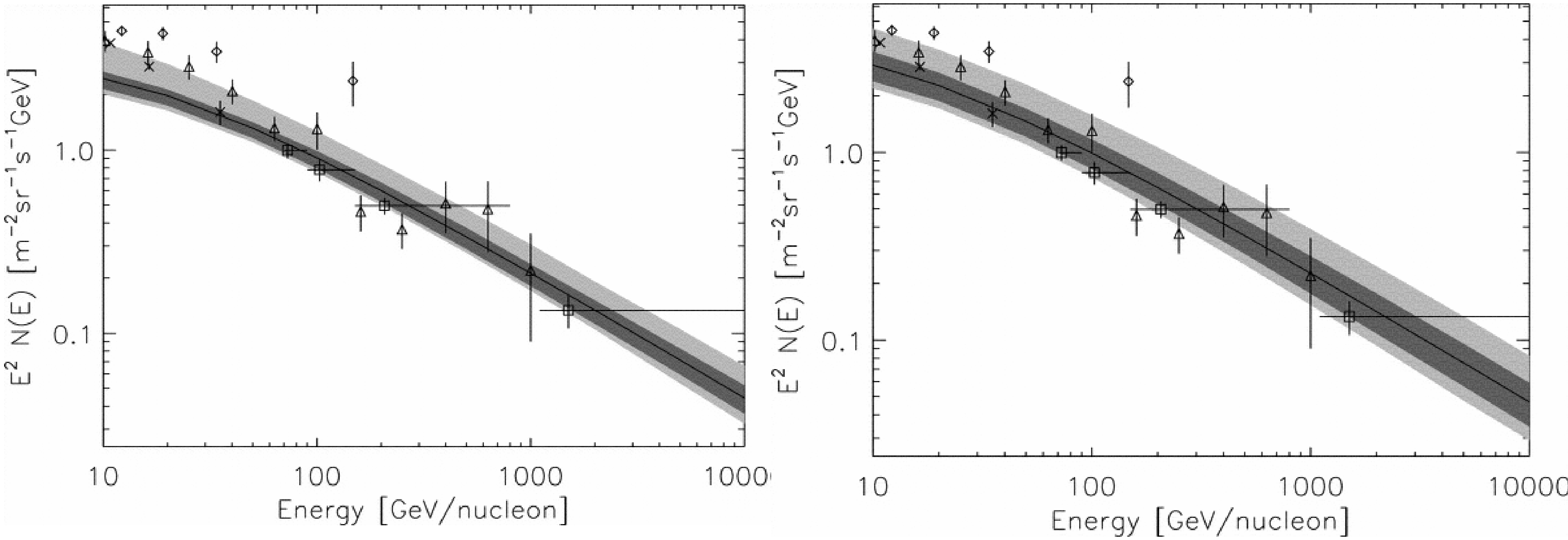

Fig.10: Same as Fig. 9, but for ^{12}C (*left*) and ^{11}B, which is assumed to be purely secondary, produced from primary ^{12}C only (*right*).

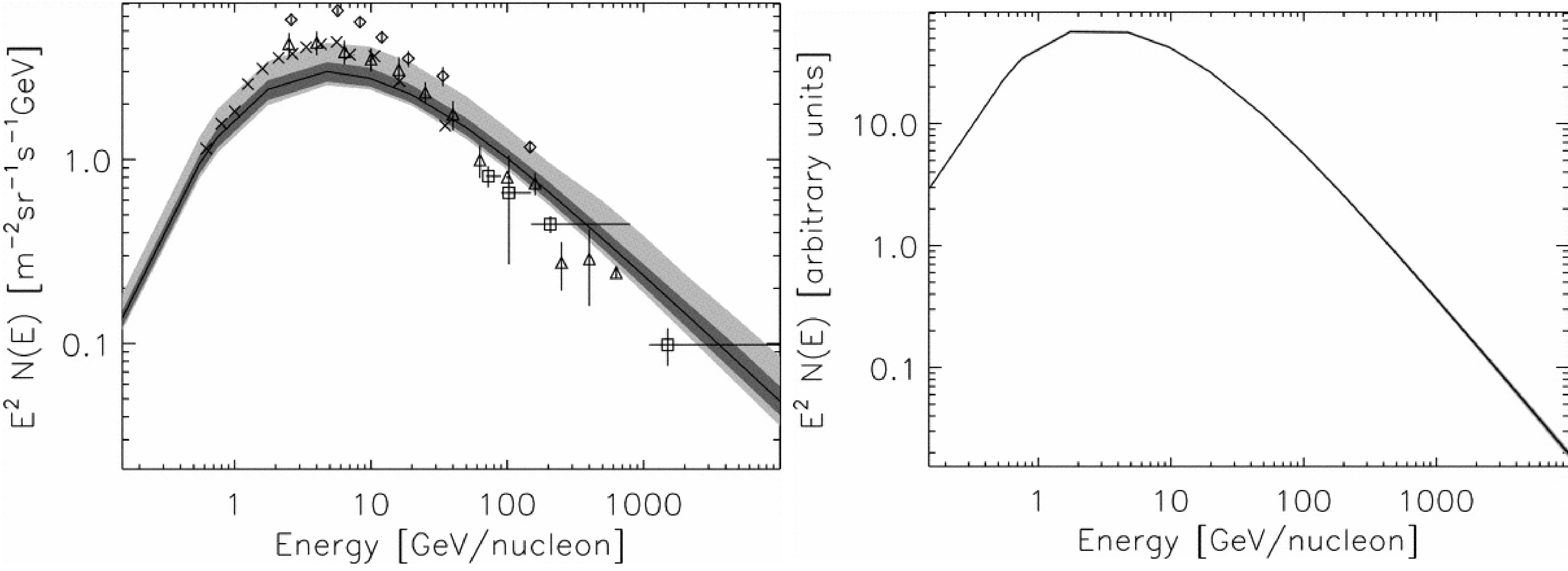

Fig.11: Sample of possible ^{12}C spectra, given at the top of the atmosphere.

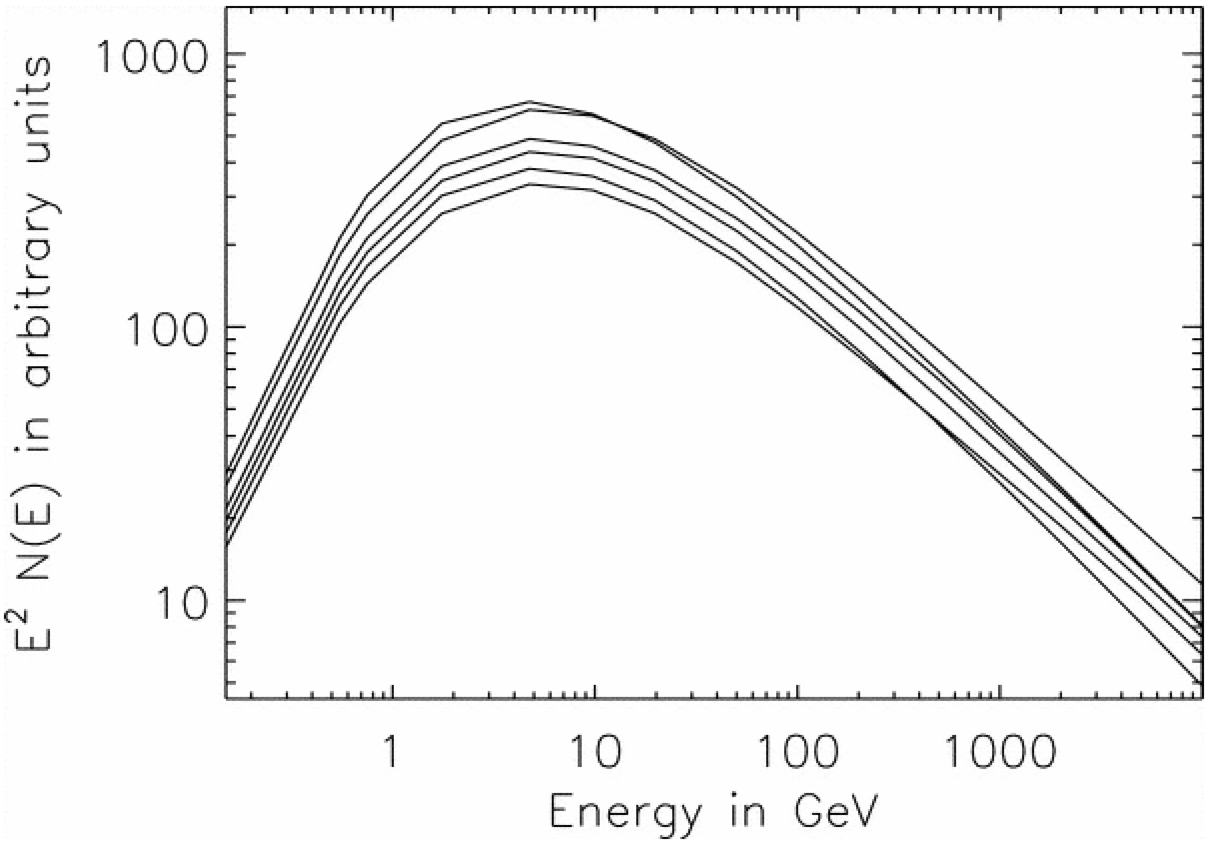

Summary

- Strong evidence that CR acceleration in SNRs leads to CR spectra that show significant variations in space and time. The behavior of the CR nuclei resembles that of protons, but differs considerably from that of CR electrons (Pohl & Esposito 1998).
- Strong variations of the CR nuclei flux, typically 20%, with occasional spikes of much higher amplitude, but only minor changes in the spectral distribution. The locally measured primary CR spectra fit well into the obtained range of possible spectra. The spectra of the secondary element boron show almost no variations, so the above findings also imply significant fluctuations of the boron-to-carbon ratio.
- Therefore, the commonly used method of determining CR propagation parameters by fitting secondary-to-primary ratios appears flawed on account of the variations that these ratios would show throughout the Galaxy.
- γ-ray observations of the outer Galaxy show suggests an enhancement of the CR density in the Perseus arm (Digel et a. 2001), which would be well explained by the variations in the flux of CR nuclei that results from an SNR origin.

S. Digel et al., ApJ 555, 12 (2001)

“EGRET OBSERVATIONS OF MONOCEROS: DIFFUSE GAMMA-RAY EMISSION IN THE OUTER GALAXY”

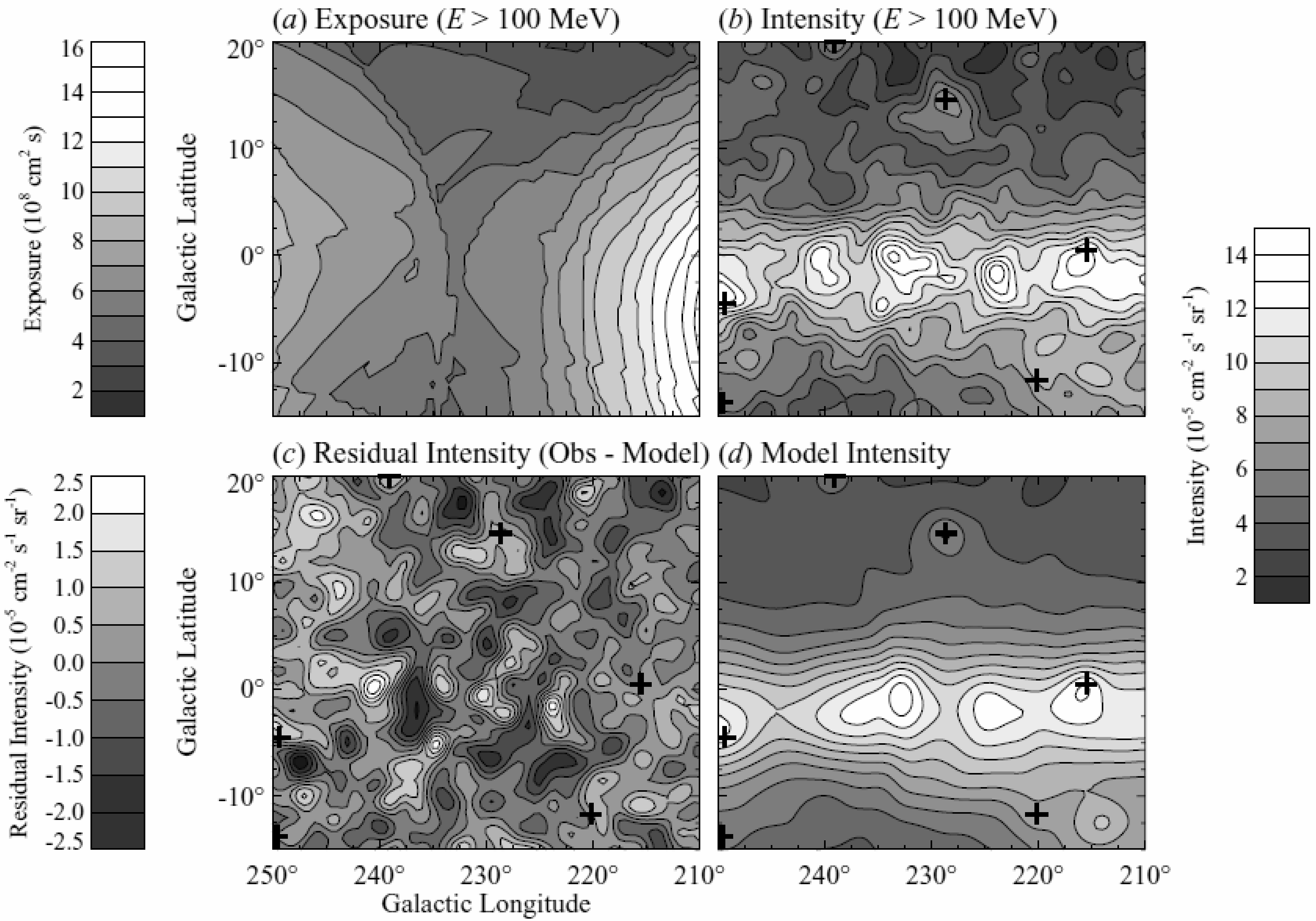

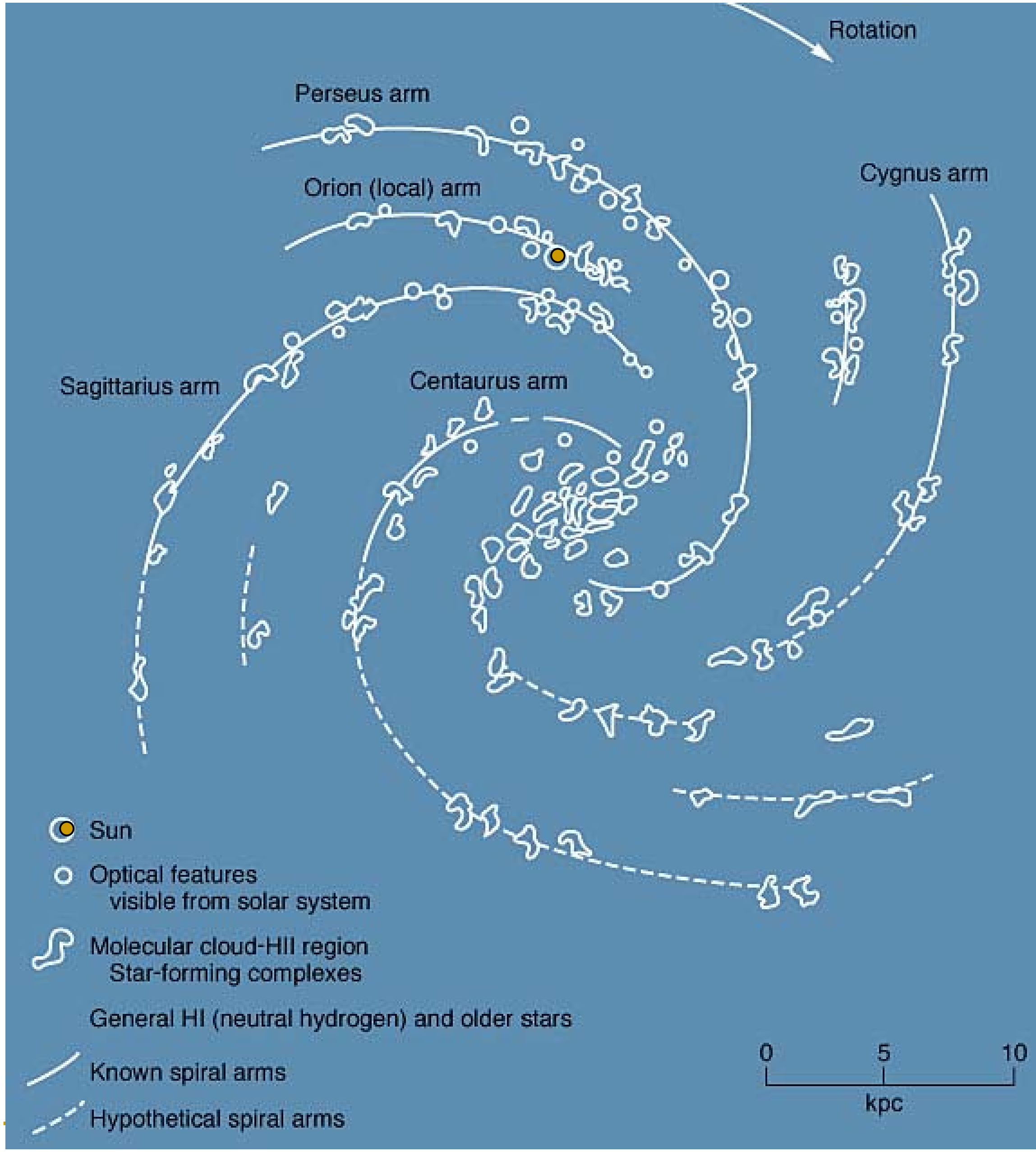

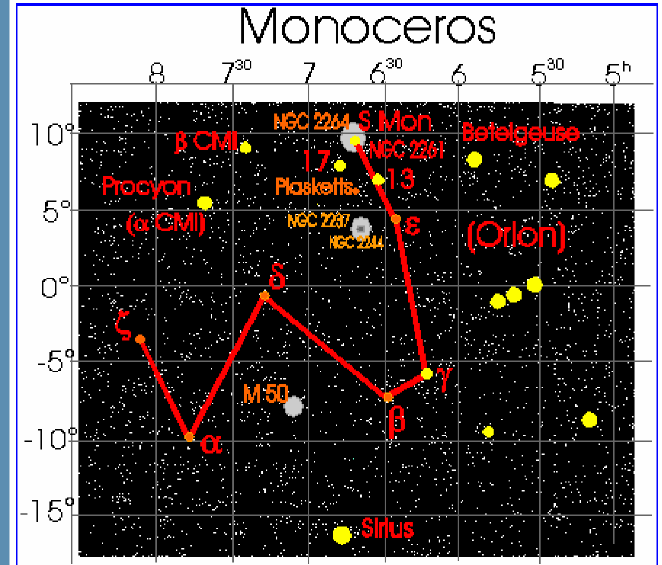

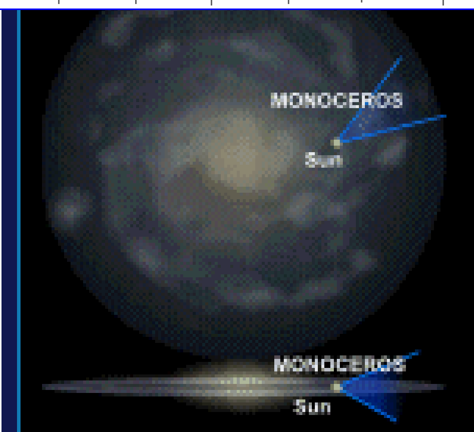

Monoceros lies next to Orion on the band of the Milky Way, and so the area of space it describes is on the plane of our Galaxy. Much of the Milky Way visible in this constellation belongs to the Orion Arm of the Galaxy.

S. Digel et al., ApJ 555, 12 (2001)

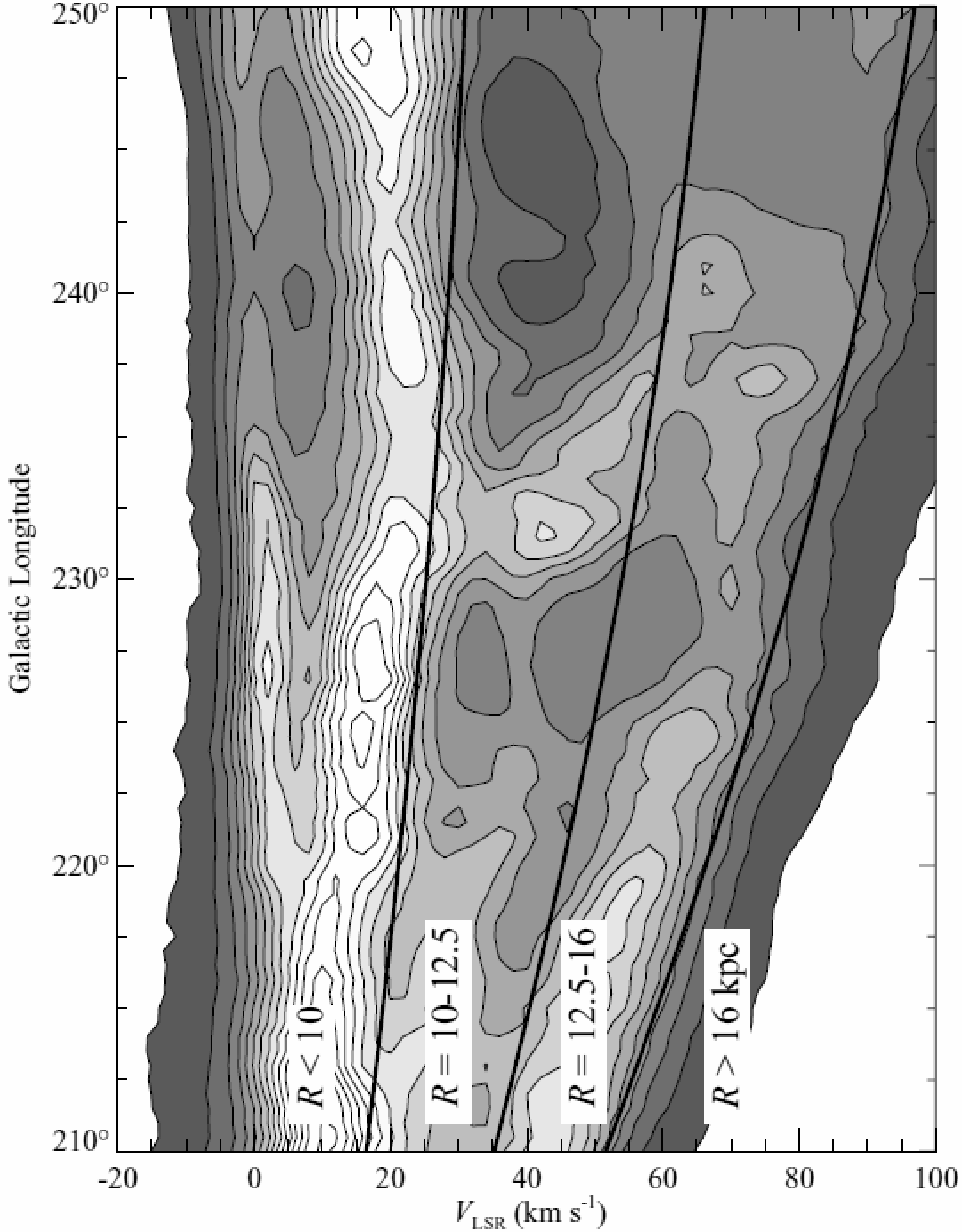

FIG. 1.—Longitude-velocity diagram of the average intensity of 21 cm H I emission for $|b| < 15°$ in Monoceros. The H I data are from the surveys cited in the text. The lowest contour is 1.5 K, and the contour interval is 3 K. On the assumption of circular rotation, thick lines denote the boundaries between the four annuli of Galactocentric distance used in the analysis of the diffuse emission: (1) $R < 10$ kpc, (2) $R = 10$–12.5 kpc, (3) $R = 12.5$–16 kpc, and (4) $R > 16$ kpc.

S. Digel et al., ApJ 555, 12 (2001)

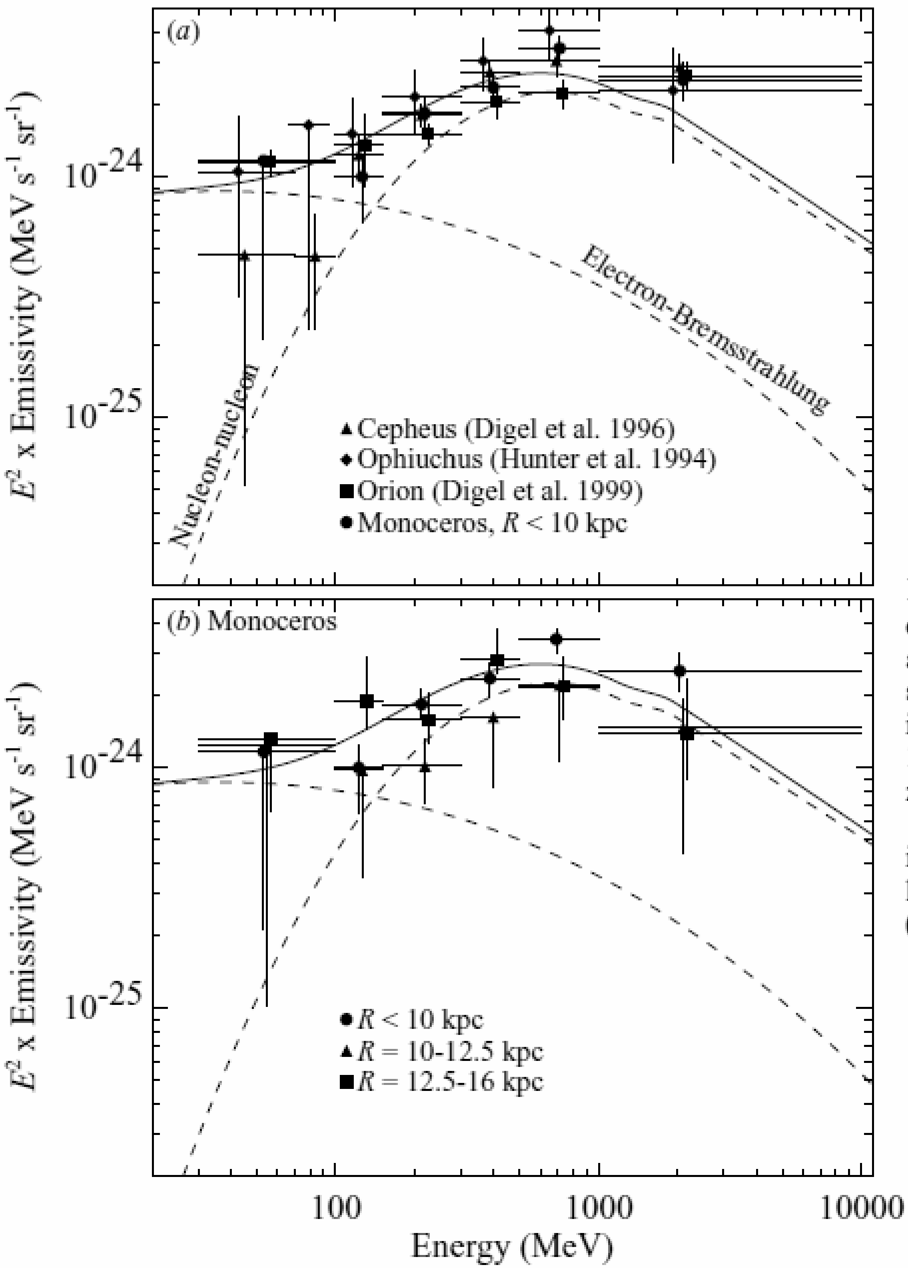

FIG. 6.—(*a*) Comparison of differential emissivities for the local gas in Monoceros (*circles*; Table 3) with emissivities from other studies of local clouds: Ophiuchus (*diamonds*; Hunter et al. 1994), Orion (*squares*; Digel et al. 1999), and Cepheus (*triangles*; Digel et al. 1996). (*b*) Differential emissivities in the three inner annuli in Monoceros derived from the coefficients in Table 3. *Circles*: local ($R < 10$ kpc) range; *triangles*: interarm ($R = 10$–12.5 kpc) range; and *squares*: Perseus arm ($R = 12.5$–16 kpc) range. Horizontal error bars indicate the energy range and the vertical error bars the $\pm 1\ \sigma$ uncertainty in the emissivity. For upper limits, the 2 σ values are indicated. Also plotted are the nucleon-nucleon and electron-bremsstrahlung emissivities and their sum for the solar vicinity from Bertsch et al. (1993).